eppendorf

Most Compact

QbD-driven process development with the DASbox® Mini Bioreactor System

With working volumes of 60 – 250 mL the DASbox is the optimal tool for advanced cell culture and microbial process development and Design of Experiments (DoE) applications. All critical parameters can be precisely controlled.

- > Parallel set-up of up to 24 bioreactors
- > Perfectly suited for microbial and cell culture applications
- > Liquid-free exhaust condensation
- > Fully mass flow-controlled gas mixing
- > Available with single-use vessels

New: Designed for stem cell process development: BioBLU® 0.3sc with 8-blade impeller

www.eppendorf.com/DASbox

Received: 13 November 2019 | Revised: 28 May 2020 | Accepted: 20 June 2020

DOI: 10.1002/bit.27470

ARTICLE

BIOTECHNOLOGY BIOENGINEERING WILEY

Virus harvesting in perfusion culture: Choosing the right type of hollow fiber membrane

Alexander Nikolay[1] | Joris de Grooth[2] | Yvonne Genzel[1] | Jeffery A. Wood[3] | Udo Reichl[1,4]

[1]Bioprocess Engineering, Max Planck Institute for Dynamics of Complex Technical Systems, Magdeburg, Germany

[2]Films in Fluids, University of Twente, Enschede, The Netherlands

[3]Soft Matter, Fluidics and Interfaces, Faculty of Science and Technology, MESA+ Institute for Nanotechnology, University of Twente, Enschede, The Netherlands

[4]Chair for Bioprocess Engineering, Otto-von-Guericke-University Magdeburg, Magdeburg, Germany

Correspondence
Yvonne Genzel, Bioprocess Engineering, Max Planck Institute for Dynamics of Complex Technical Systems, Magdeburg, Germany.
Email: genzel@mpi-magdeburg.mpg.de

Present address
Alexander Nikolay, Univercells SA, Brussels, Belgium.

Abstract

The use of bioreactors coupled to membrane-based perfusion systems enables very high cell and product concentrations in vaccine and viral vector manufacturing. Many virus particles, however, are not stable and either lose their infectivity or physically degrade resulting in significant product losses if not harvested continuously. Even hollow fiber membranes with a nominal pore size of 0.2 µm can retain much smaller virions within a bioreactor. Here, we report on a systematic study to characterize structural and physicochemical membrane properties with respect to filter fouling and harvesting of yellow fever virus (YFV; ~50 nm). In tangential flow filtration perfusion experiments, we observed that YFV retention was only marginally determined by nominal but by effective pore sizes depending on filter fouling. Evaluation of scanning electron microscope images indicated that filter fouling can be reduced significantly by choosing membranes with (*i*) a flat inner surface (low boundary layer thickness), (*ii*) a smooth material structure (reduced deposition), (*iii*) a high porosity (high transmembrane flux), (*iv*) a distinct pore size distribution (well-defined pore selectivity), and (*v*) an increased fiber wall thickness (larger effective surface area). Lowest filter fouling was observed with polysulfone (PS) membranes. While the use of a small-pore PS membrane (0.08 µm) allowed to fully retain YFV within the bioreactor, continuous product harvesting was achieved with the large-pore PS membrane (0.34 µm). Due to the low protein rejection of the latter, this membrane type could also be of interest for other applications, that is, recombinant protein production in perfusion cultures.

KEYWORDS

cell culture-based virus production, hollow fiber membrane, perfusion, SEM

Abbreviations: ATF, alternating tangential flow filtration; BGM, basal growth medium; BHK-21$_{SUS}$, suspension-adapted baby hamster kidney cell; D_{90}, measured particle cutoff in µm; dH_2O, deionized water; dsDNA, double-stranded DNA; DSP, downstream processing; ID, inner fiber diameter in mm; mPES, modified polyethersulfone; PE, polyethylene; PES, polyethersulfone; PFU, plaque forming unit in PFU/ml; PS, polysulfone; PS cell, stable porcine cells; TFF, tangential flow filtration; TMP, transmembrane pressure in mbar; YFV, yellow fever virus.

1 | INTRODUCTION

Viral vaccine and viral vector production can be intensified by cultivating animal cells in perfusion mode. The increased cell concentration allows for higher virus titers. To retain cells in the bioreactor vessel, cell retention devices are required that are typically classified by their physical separation principle such as filtration, sedimentation, ultrasonic fixation, or dielectrophoretic exclusion (Castilho & Medronho, 2002). Due to their scalability, simplicity, and efficient cell retention, hollow fiber-based systems are today widely applied for manufacturing of recombinant proteins (Bielser, Wolf, Souquet, Broly, & Morbidelli, 2018). In addition, there is a growing interest for their use in the production of viral vaccines (Gallo-Ramirez, Nikolay, Genzel, & Reichl, 2015; Tapia, Vázquez-Ramírez, Genzel, & Reichl, 2016). With increasing cell concentrations, larger quantities of viruses and other particles are typically released into the medium. In contrast to recombinant protein production, virus infection triggers cell apoptosis, which results in cell degradation and lysis increasing the overall burden of impurities. Besides virus particles and extracellular vesicles, high amounts of DNA and proteins can accumulate. During continuous harvesting this can cause pore narrowing and eventually membrane blockage. In the recent years, numerous studies have reported on such unwanted filter fouling even when large-pore hollow fiber membranes have been applied (Bolton & Apostolidis, 2017; Genzel et al., 2014; Nikolay, Castilho, Reichl, & Genzel, 2018; Nikolay, Léon, Schwamborn, Genzel, & Reichl, 2018; Walther, McLarty, & Johnson, 2018; S. Wang et al., 2017). Product retention was in each case correlated to filter fouling, but a systematic characterization of membrane properties and the performance of retention devices in virus particle harvesting is still missing.

Membrane fouling is studied intensively for downstream processing (DSP), but only a very limited number of studies was performed regarding the use of membranes in upstream processing, that is, for perfusion cultivations. However, product retention has gained more attention as novel production systems aim towards process intensification and continuous biomanufacturing. Three mechanisms are mainly relevant for filter fouling leading to a reduced transmembrane flux and increased membrane resistance (Trzaskus, de Vos, Kemperman, & Nijmeijer, 2015):

(1) Internal fouling: adsorption of membrane-compatible particles to the filter material leading to pore narrowing (particle size < pore size);
(2) Partial or complete pore blocking: steric pore clogging with particles or agglomerates (particle size ~ pore size);
(3) Gel/cake layer formation: additional solute layer formation of larger particles on top of the membrane by adsorption and subsequent compression by smaller particles (particle size > pore sizes).

While internal fouling typically narrows pore channels, pore blockage, and cake layer formation equally contribute to a reduction in the effective membrane cutoff leading to membrane blockage and filtration termination. The fouling behavior of a hollow fiber module is closely associated with the properties of the membrane, in particular, its pore size distribution, porosity, surface and material roughness, and inner membrane surface charge. Overall properties do not only depend on the specific membrane material used, but also on fabrication procedures and postmodifications (Cornelissen, 1997; Rana & Matsuura, 2010; Ulbricht, Richau, & Kamusewitz, 1998). Due to the high complexity of cell culture processes (e.g., large variation in particles sizes, different surface charges and concentrations, and diverse transport properties), the description of fouling is typically limited to (semi-)empirical models.

Besides the choice of the membrane, specific operational strategies can be established to minimize the risk of filter blockage that take additionally into account the shear sensitivity of animal cells (Futselaar, 1993). First, concentration polarization and boundary layer resistances should be reduced to increase mass transfer coefficients. This can be achieved by increasing the cross-flow velocity (resulting in higher Reynolds numbers) in the filter lumen (e.g., higher flow rate and smaller hollow fiber diameter) or by reducing the transmembrane flux (e.g., lower permeate flow rate and increased membrane area). Another option is the inversion of the tangential flow filtration (TFF) direction resulting in an alternating (bidirectional) tangential flow (ATF). At a given frequency using high flow pulses, this increases the Reynolds number and potentially vortex formation so that foulants are removed more effectively. Second, hydraulic backflushing can be considered by reversing the permeate flow direction across the membrane. This can lift loose deposits on the membrane surface (Hiller, Clark, & Blanch, 1993; Kelly et al., 2014). Likewise, fast inversions of the feed flow direction, as described for ATF systems, can be applied. Thereby, membrane sections along the fiber change periodically the flow direction across the membrane facilitating continuous backflushing with each pump cycle (Radoniqi, Zhang, Bardliving, Shamlou, & Coffman, 2018; Figure 1). Although these hydraulic cleaning methods can be effective, they may increase the shear stress on cells and reduce the net flux. Therefore, it is much more favorable to select a membrane where little fouling occurs, and a stable flux can be easily maintained to reduce the number of hydraulic cleaning steps.

In this study, we investigated different membrane materials and their properties for continuous virus particle harvesting via the permeate for perfusion cultivation. To cover a large variety of different commercial hollow fiber membranes, polyethersulfone (PES), modified PES (mPES), polysulfone (PS), mixed ester (ME, consisting of cellulose acetate and cellulose nitrate), and polyethylene (PE) membranes were tested. If available, two pore sizes (based on nominal cutoff) were investigated to either retain or harvest the virus particles over the cultivation period and to understand filter fouling in dependence of the pore size. This resulted in a sample set of eight hollow fiber modules.

We first characterized different hollow fiber membranes with respect to their potential fouling behavior. In a second step, we tested the membranes in TFF operation for filter fouling and virus particle harvesting. For this, suspension-adapted baby hamster kidney (BHK-21$_{SUS}$) cells were cultured in a bioreactor with an external

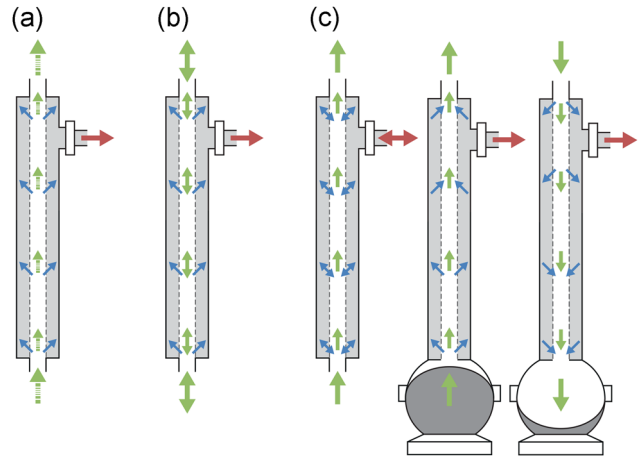

FIGURE 1 Minimizing filter fouling during perfusion cultivations. (a) A typical unidirectional flow (TFF) can counter fouling by increased/pulsed inlet flow velocity (green dotted arrow). (b) Inversion of flow direction results in a bidirectional tangential flow supporting the removal of foulants (green double arrow). (c) Hydraulic backflushing can be achieved by inverting the permeate flow (red double arrow). A similar effect of reversed transmembrane flow (blue arrow) along the membrane is described for certain membrane lengths and diaphragm pumps such as the XCell™ ATF from Repligen [Color figure can be viewed at wileyonlinelibrary.com]

TFF cell retention device (recirculation loop), and the cells were subsequently infected with yellow fever virus (YFV; ~50 nm). Filter fouling was monitored in real time using transmembrane pressure sensors, and virus particle, DNA, and protein concentrations were measured in the permeate flow to relate membrane structure measurements to process performance.

2 | MATERIALS AND METHODS

2.1 | Hollow fiber membranes

Eight commercial hollow fiber membranes (Table 1) were characterized and tested for filter fouling in unidirectional TFF operation.

2.2 | Pore size distributions

To determine pore size distributions, a dry single hollow fiber (50 mm length) was potted with a hot glue gun into a PE tubing (5 mm inner diameter [ID]). The end of the fiber was closed with glue and subsequently wetted with the pore-filling liquid fluorinert FC-43 (3 M). The pore size distribution was measured with a Porolux 500 (Porometer) following the method described by Trzaskus et al. (2015). Based on the measured pore size distribution, the exclusion limits (cutoffs) of the membranes were calculated as defined to retain 90% of a minimum particle size (relates to the cumulative distribution at 90%; in short D_{90}). To evaluate the pore size distribution, the width was determined at the 90th percentile (relates to the range from D_5 to D_{95}) eliminating measurement noise at lowest and highest pore sizes.

2.3 | Membrane surface charge

To determine the zeta potential of the inner membrane surface, a single hollow fiber (90 mm length) was potted in a PE tube (80 mm length and 5 mm ID) filled completely with two-component epoxy resin and dried overnight. Protruding glued ends were cut and the potted membrane was mounted between clamping cells of a SurPASS electrokinetic

TABLE 1 Hollow fiber filter modules tested for filter fouling and virus retention in tangential flow filtration (TFF) operation

# Material	Effective length (mm)	Surface area[a] (cm^2)	Inner diameter (mm)	Number of fibers per module	Fiber wall thickness[b] (mm)	Flow velocity[c] (mm/s)
1 mPES	200	20	0.5	6	0.15	125
2 mPES	200	15	0.7	3	0.15	175
3 PES	200	28	0.5	9	0.10	125
4 PES	200	13	1.0	2	0.10	250
5 PS	200	28	0.5	9	0.13	125
6 PS	250	50	1.4	5	0.45	350
7 ME	200	20	0.6	5	0.15	150
8 PE	200	45	7.3	1	2.75	1,825

Note: Product names and nominal pore sizes as provided by suppliers are not disclosed due to confidentiality agreements.

Abbreviations: ME, mixed ester; mPES, modified polyethersulfone; PE, polyethylene; PES, polyethersulfone; PS, polysulfone.

[a]Surface area as stated by suppliers.

[b]Measured with digital vernier caliper with a standard error of ±0.05 mm.

[c]Flow velocity in fibers differed among hollow fiber modules to operate all filtration experiments at a fixed shear rate.

analyzer (Anton Paar). The streaming potential of membranes was measured in a 5 mM KCl electrolyte solution at a pH of 7.2 (±0.1). The zeta potential was calculated from the streaming potential via the Fairbrother–Mastin equation (Fairbrother & Mastin, 1924).

2.4 | Cell broth zeta potential

The zeta potential of the crude cell broth was measured in triplicates using 1.5 ml samples filled in a folded capillary zeta cell using a the Zetasizer Nano ZS (Malvern Instruments). The cell culture medium was measured as dispersant with a refractive index (RI) of 1.33, based on refractometry measurements (RE40D Refractometer, Mettler Toledo). Assuming a very low Debye length relative to the size of the colloids in the broth, the Smoluchowski approximation was used to calculate the zeta potential based on the electrophoretic mobility (Swan & Furst, 2012), and each sample was measured 30 times at 25°C following the manufacturer's recommendations.

2.5 | Scanning electron microscopy

Native and fouled membranes were either cut manually or frozen in liquid nitrogen before being broken manually. In brief, membrane fractions were fixed with carbon conductive tapes and carbon paint (DAG-T-502, Ted Pella) on specimen mounts, and vacuum-dried at 30°C overnight. A 10 nm chromium layer was sputtered on the sample with a Quorum Q150T ES (Quorum). The cross-section and surface morphology of the membranes was obtained using a scanning electron microscope (SEM; JSM-6010LA, JOEL) at 5 kV.

2.6 | Membrane filtration setup and experiment

Suspension-adapted BHK-21$_{SUS}$ cells (derived from adherent BHK-21 cells, kindly provided by Dr. Boris Hundt, IDT Biologika) were cultivated in serum-free basal growth medium (BGM) in a 2.5 L DasGip glass bioreactor connected to a DasGip DCU controller (Eppendorf). Cells were infected with YFV-17D (kindly provided by Prof. Dr. Mathias Niedrig, Robert Koch Institute Berlin) at multiplicity of infection of 10^{-1} based on the plaque assay as described below. All membranes were prewetted with deionized water (dH_2O), subsequently gently drained and connected to an external recirculation loop with a peristaltic pump (Watson–Marlow 120U). The membranes were consecutively tested in TFF mode at a fixed shear rate (γ) of 2,000 s^{-1}. Therefore, volumetric flow rates $\dot{V}_f$ (ml/min) were adjusted based on the cross-sectional areas of all fibers of each module:

$$\dot{V}_f = \frac{f_n \bullet \pi \bullet r^3 \bullet \gamma}{4} \quad (1)$$

where f_n is the number of hollow fibers and r the inner fiber lumen radius of individual fibers (mm). The permeate pump was set to a permeate flux rate J of about 33 L/hr/m^2 describing the ratio of the permeate flow rate $\dot{V}_p$ (L/hr) to the total filtration surface area A (m^2) of all fibers in one module:

$$J = \frac{\dot{V}_p}{A} \quad (2)$$

The permeate was transferred back into the bioreactor. Inlet, outlet, and permeate pressure were measured with inline single-use PS pressure transducers (either TC or luer lock, ACPM-799-01N, Spectrum Labs). Transducers were connected to a digital pressure monitor (KrosFlo Digital Pressure Monitor, Spectrum Labs) or to the peristaltic pump controller (KR2i, Spectrum Labs) to record data at 5 s sampling intervals (Excel sheet KF Comm Complaint Workbook with interface software package from Ofni Systems). The total resistance (R, m^{-1}) was calculated based on Darcy's law:

$$R = \frac{\mathrm{TMP}}{\eta_m \bullet J} \quad (3)$$

where TMP is the transmembrane pressure (mbar) and η_m the dynamic viscosity of the medium (0.69 mPa s at 37°C). With the inlet equal to the outlet pressure, the TMP corresponds to the pressure difference between the feed and permeate stream. The fouling capacity of each membrane was described by the specific permeate volume V_p (L/m^2) as

$$V_p = \frac{\mathrm{V}}{A} \quad (4)$$

with V as maximum permeate volume (L).

Samples of the bioreactor vessel and the permeate line were taken regularly, centrifuged at 2,000×g for 3 min and optionally stored at −80°C until use. The pH of the cell broth was measured with a pH probe (405 DPAS SC K8S, Mettler Toledo), the osmolality with the Vapro 5520 pressure osmometer (Wescor), and the turbidity at 880 nm with a turbidity Dencytee probe (Hamilton). The cell concentration, cell diameter, and cell viability (based on trypan blue exclusion) were determined with an automated cell counter (ViCell XR, Beckman Coulter) from a total number of 100 images per measurement.

2.7 | Virus quantification

Infectious YFV titers were quantified by plaque assay using stable porcine (PS) cells as described previously (Nikolay et al., 2018). In brief, PS cells were seeded as monolayer into 24-well plates and infected with diluted virus samples. A viscous overlay was added and after an incubation period of 3 days, virus-induced plaques were counted. Virus titers were expressed as plaque-forming units per volume (PFU/ml) with a coefficient of variation of 15%.

2.8 | DNA and protein quantification

Protein and double-stranded (ds) DNA concentrations were estimated using the Bradford assay (in triplicates) and the PicoGreen assay (in

duplicates) as described elsewhere (Wickramasinghe, Kalbfuß, Zimmermann, Thom, & Reichl, 2005). In brief, bioreactor and permeate samples were centrifuged at 2,000×*g* for 2 min at 4°C. The supernatant was inactivated at 80°C for 2 min and by overnight incubation with 0.5% (*v/v*) formaldehyde at 4°C. Protein samples were diluted in dH_2O and well mixed with Coomassie brilliant blue (Quick Start Bradford Protein Assay, Bio-Rad) in transparent flat bottom 96-well microtiter plates. The maximum of the absorption spectrum was measured at 595 nm (InfiniteM 200 PRO). For dsDNA quantification, PicoGreen dye (Quant-iT PicoGreen dsDNA Assay Kit, Thermo Fisher Scientific) was added to the sample and mixed well. Subsequently, samples were excited at 480 nm and the fluorescence emission intensity measured at 520 nm (InfiniteM 200 PRO). A standard solution was prepared from lambda DNA (D1501, Promega).

2.9 | Rejection coefficient

The rejection coefficient σ_{reject} was introduced to describe the fraction of product retained by the membrane and calculated as

$$\sigma_{reject} = 1 - \frac{C_p}{C_v} \quad (5)$$

where C_p is the YFV (PFU/ml), DNA or protein concentration (μg/ml) in the permeate flow, and C_v (PFU/ml or μg/ml) the respective concentration in the bioreactor vessel.

3 | RESULTS

3.1 | Structural and physicochemical membrane properties

The fiber wall thickness of most hollow fiber membranes was in a range between 0.10 and 0.15 mm, whereas large-pore PS (#6) and PE (#8) membranes were significantly thicker with 0.45 and 2.75 mm (Table 1).

Pore size distributions of membranes were determined by capillary flow porometry. The membrane-specific exclusion limit (cutoff) of the cumulative pore size distribution at 90% (relates to D_{90}) ranged from 0.08 μm to 1.69 μm (Table 2). Interestingly, the measured pore sizes differed from manufacturer's specifications. Compared with nominal pore sizes (cannot be provided due to confidentiality agreements) four membranes had a larger effective cutoff by factors between 0.2 and 5.9, and four a smaller effective cutoff by factors of 0.1–0.8 (not shown here).

The width of the pore size distribution was described with the pore size width at 90th percentile and expressed in relation to the measured cutoff. Large-pore PE membranes tended to have a broader pore size width, while the PS membranes had very distinct pore sizes (Table 2; Figure S1).

Next, all membranes were examined with SEM imaging to investigate structural details. The material roughness was mainly assessed based on the frontal view of the inner membrane (Figures 2 and S2). While a highly jagged material surface was found for the large-pore mPES fiber, the roughness decreased from ME, PES (0.18 μm), PS (0.08 μm) materials to very smooth PS (0.34 μm), and PE structures. In addition, the porosity of the inner surface was qualitatively evaluated. SEM imaging revealed a remarkably high surface porosity for the PS (0.34 μm) membrane, which decreased from ME, the two PES, and the PE to the PS (0.08 μm) membrane. Due to the highly jagged material, visual evaluation of the mPES membrane was difficult. However, funnel-shaped pores were present, as equally observed for the PE membrane turning both membranes potentially susceptible for rapid particle entrapment.

Subsequent cross-section and frontal SEM imaging of the inner membrane helped to characterize surface roughness and overall porosity (Figures S3 and S4). The mPES membrane had a very high surface roughness with distinct and deep valleys. The PES (0.18 μm) and ME membranes, whereas, had a flatter inner surface structure than the PS (0.34 μm), and PE membranes revealing a wavy surface. The mPES material had a high porosity, followed by decreasing porosities with the large-pore PS, ME, PES, PE, and finally small-pore PS membranes. In particular, the front view of the outer surface revealed a strong asymmetric structure for most membranes except for the PE membrane (Figure S4). A closer examination of the large-pore PS membrane revealed a high overall porosity in the first inner half, which then became more compact to the outer side (Figure S5).

Finally, the electrokinetic potential of membranes and potential foulants was assessed. First, the streaming potential of each membrane material was measured at pH 7.2 and 5 mM KCl solution to calculate the zeta potential. The zeta potential was about −24 mV for most materials, whereas the mPES material showed a slightly lower surface charge with −19.7 mV (Table S1). Then, the zeta potential of the culture broth containing infected cells (with extracellular vesicles, virions, and debris) was calculated. Based on the electrophoretic

TABLE 2 Overview on measured cutoff and pore size width (indicates pore size distribution) of hollow fiber membranes

# Material	Cut-off (μm; D_{90})[a]	Pore size width (μm)[b]
1 mPES	0.09	0.03 (33%)
2 mPES	1.08	0.51 (47%)
3 PES	0.18	0.04 (22%)
4 PES	0.37	0.16 (43%)
5 PS	0.08	0.01 (13%)
6 PS	0.34	0.07 (21%)
7 ME	0.25	0.07 (28%)
8 PE	1.68	1.87 (111%)

Abbreviations: ME, mixed ester; mPES, modified polyethersulfone; PE, polyethylene; PES, polyethersulfone; PS, polysulfone.
[a]Measured cutoff for a cumulative distribution at 90%.
[b]Pore size width at 90th percentile of pore size distribution (value in brackets expresses width in percentage to cutoff).

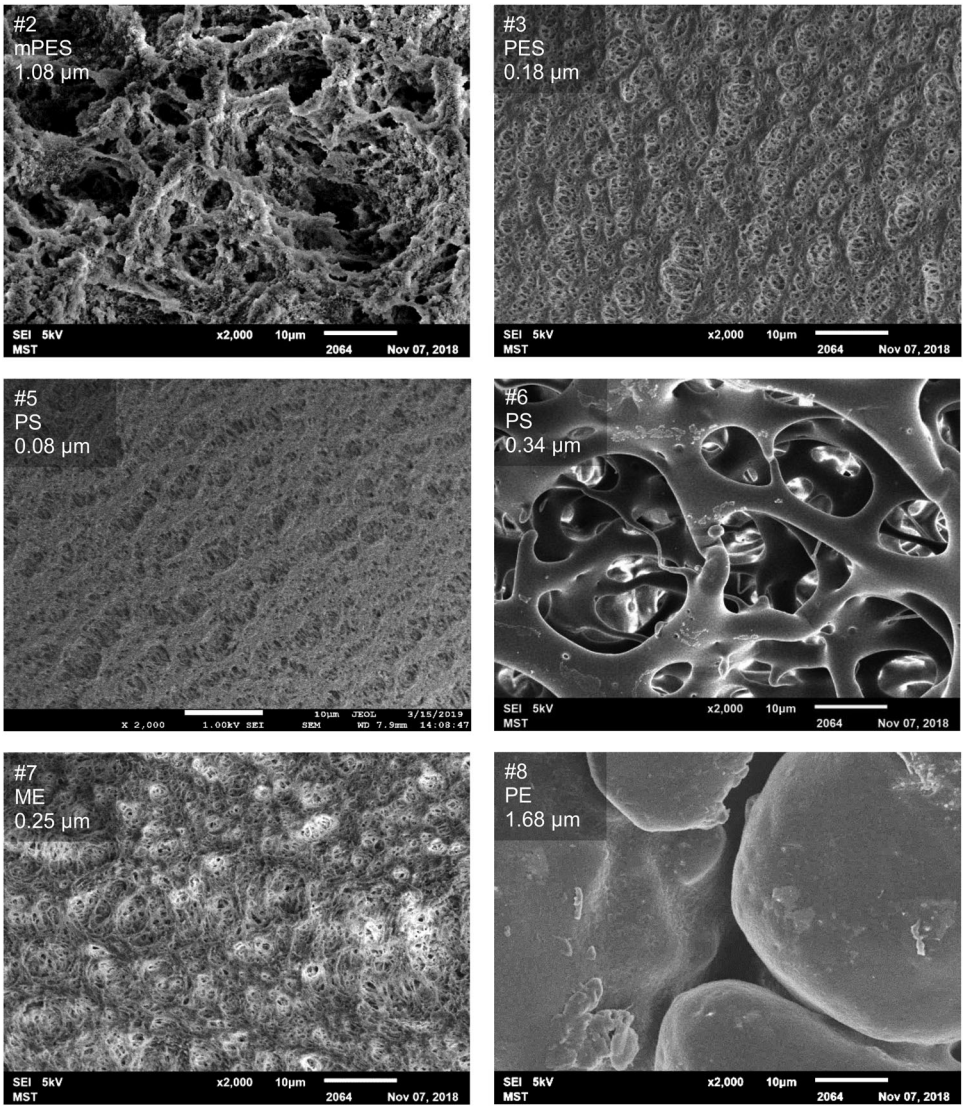

FIGURE 2 SEM images of the inner membrane surface of different hollow fiber materials. At given scale, a ×2,000-fold magnification allowed direct comparison of roughness, surface structure, and porosity of unused membranes. ME, mixed ester; mPES, modified polyethersulfone; PE, polyethylene; PES, polyethersulfone; PS, polysulfone; SEM, scanning electron microscope

mobility of all particles, a zeta potential of −16.4 ± 0.4 mV was determined at pH 7.2 and ionic strength of the cell broth.

3.2 | Filter fouling in TFF perfusion mode

In this study, a set of process conditions suitable for perfusion operation with animal cell culture was defined and applied to all membranes as a direct one-to-one comparison. Thereby, effective membrane lengths of 200–250 mm, relatively high flow velocities of 125 mm/s or larger (in accordance to a fixed shear rate; Table 1) and fixed permeate flux of about 33 L/hr/m^2 were chosen to allow a uniform flux distribution and homogenous membrane fouling. The hollow fiber membranes (#1–#8) were tested consecutively. During filtration experiments, the infected BHK-21$_{SUS}$ cell culture had a concentration of 5.2×10^6 cells/ml with a viability of 80.2% and an average cell diameter of 15.4 µm. The virus titer was determined to 9×10^4 PFU/ml. Protein and dsDNA impurity levels were at 255 µg/ml and 13.7 µg/ml, respectively. The cell broth had a pH of 7.2, an osmolality of 236 mmol/kg and a turbidity of 6.90 NTU$_{880}$.

During the filtration experiment, the membrane resistance increased fast for the two mPES, both PES and the ME membranes with only short periods of slower resistance development (Figure 3). At maximum technical resistance, the permeate flow dropped and the silicone tubing on the permeate side collapsed due to low pressure at permeate side. Thereby, a V_p of around 9–18 L/m^2 until termination was reached for most membranes (Table 3). For the tested PS membranes (0.08 and 0.34 µm), it took significantly longer before the maximum resistance was achieved resulting in permeate volumes of 30 L/m^2 and 75 L/m^2, respectively.

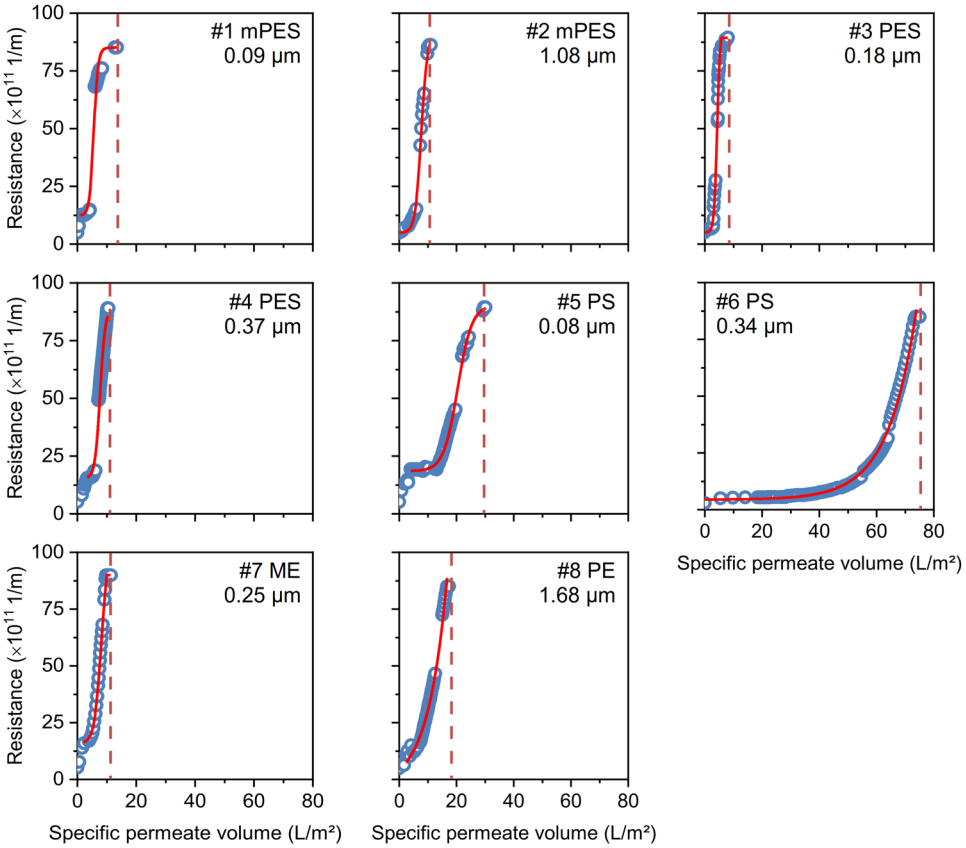

FIGURE 3 Hollow fiber membrane resistance during perfusion operation in tangential flow filtration mode. Membranes were challenged with a cell culture broth containing infected BHK-21$_{SUS}$ cells at a constant permeate flux of 33 L/m^2/hr. Filtration resistance (blue circle) increased with the specific permeate volume until reaching maximum fouling capacity. Data points were fitted using splines to visualize the development of membrane fouling. Red vertical line indicates maximum specific permeate volume until full membrane blockage. BHK-21$_{SUS}$, suspension-adapted baby hamster kidney cell; ME, mixed ester; mPES, modified polyethersulfone; PE, polyethylene; PES, polyethersulfone; PS, polysulfone [Color figure can be viewed at wileyonlinelibrary.com]

TABLE 3 Overview on maximum surface-specific permeate volumes for each hollow fiber membrane operated in tangential flow filtration mode

# Material	Cutoff (µm)	Max. specific permeate volume (L/m^2)[a]
1 mPES	0.09	13
2 mPES	1.08	11
3 PES	0.18	09
4 PES	0.37	11
5 PS	0.08	30[b]
6 PS	0.34	75[b]
7 ME	0.25	11
8 PE	1.68	18

Abbreviations: ME, mixed ester; mPES, modified polyethersulfone; PE, polyethylene; PES, polyethersulfone; PS, polysulfone.

[a]Maximum specific permeate volume was reached with the cessation of permeate flow and collapse of silicon tubing (maximum membrane resistance).

[b]Distinctly increased filtration performance; data derived from Figure 3.

Subsequently, a selection of blocked membranes was subjected to SEM imaging. In particular, the mPES, the PES, and the ME membranes exhibited strong filter cake formation. Interestingly, the large-pore PS membrane did neither show surface-related deposition nor indications of pore blockage and cake layer formation (Figure S6).

3.3 | Virus retention during TFF

While membranes were challenged, samples from the bioreactor broth and permeate were routinely taken and analyzed for infectious virus titer as well as DNA and protein concentrations. In the early filtration phase of small-pore membranes, virus titers in the permeate were already significantly reduced compared with the bioreactor vessel (9.0×10^4 PFU/ml; Figure 4). The small-pore mPES (0.09 µm) and PS (0.08 µm) membranes retained more than 99% of the infectious virus material, whereas almost 90% of the infectious material was retained by mid-pore PES (0.18 µm) and ME membranes (0.25 µm). The large-pore PS (0.34 µm), PES (0.5 µm), mPES (1.08 µm), and PE (1.68 µm) membranes were highly permeable for virus particles.

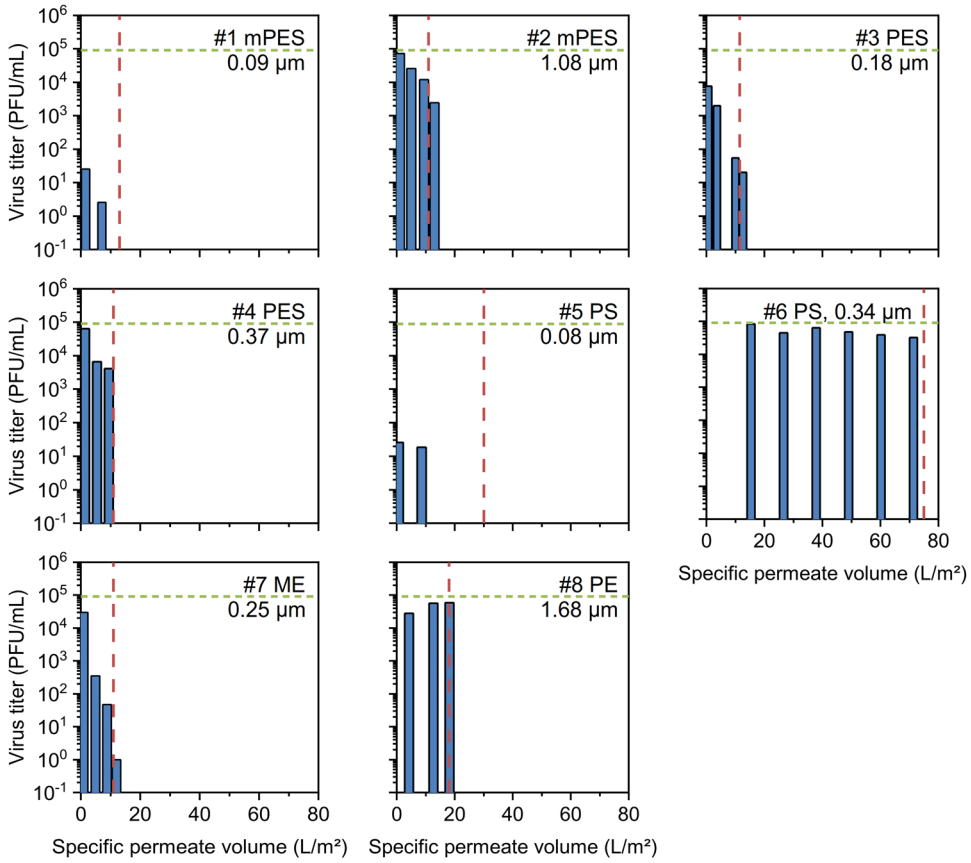

FIGURE 4 Yellow fever virus (YFV) titers in the permeate of different hollow fiber membranes tested for continuous virus harvesting during perfusion operation. BHK-21_{SUS} cells were infected with YFV and hollow fiber membranes were consecutively tested in tangential flow filtration mode. Green horizontal line indicates infectious virus titer in the bioreactor vessel (9.0×10^4 PFU/ml). Red dotted vertical line indicates complete membrane blockage. ME, mixed ester; mPES, modified polyethersulfone; PFU, plaque-forming units; PE, polyethylene; PES, polyethersulfone; PS, polysulfone [Color figure can be viewed at wileyonlinelibrary.com]

With progressing filter fouling (increasing membrane resistance), virus retention increased further for all membranes. The small-pore membranes retained the virus fully (below the limit of detection of about 10 PFU/ml), while fouling for the PS membrane (0.08 µm) was notably delayed. For the mid-pore membranes, viral titers decreased in the permeate below 1%. For the large-pore group, that is, PES (0.5 µm) and mPES (1.08 µm) membranes, virus titers in the permeate rapidly decreased to ~10%. In contrast, fouling of the PS membrane (0.34 µm) developed only slowly and the membrane remained highly permeable for infectious virions. At the end of the filtration experiment, a high fraction of virions still passed the membrane (about 35%).The PE membrane with largest pores (1.68 µm) did not retain significant virus amounts, but despite the pore size a compete membrane blockage occurred unexpectedly early (18 L/m^2).

3.4 | DNA and protein rejection

The rejection of DNA and protein contaminants was calculated based on depletion levels from the supernatant of infected BHK-21_{SUS} cells growing in BGM medium compared with the permeate (Figure 5). Similar to decreasing virus titers, the small-pore mPES and small-pore PS membranes revealed an initially high rejection for protein and, in particular, for DNA impurities. Notably, as the membrane resistance evolved slower for the PS membrane, a high specific permeate volume with reduced DNA levels of 97% (equals to < 0.2 µg/ml) was maintained. In addition, it showed the highest protein rejection of 75% with a reduced protein load of about 70 µg/ml in the permeate flow. Mid-pore size range membranes showed a similar behavior with increasing rejection rates with evolving membrane resistance and fouling. Interestingly, the PE (1.68 µm) and PS membranes (0.34 µm) showed high rejection rates in the beginning, which then stabilized with a rejection coefficient of about 10% (Figure 5).

4 | DISCUSSION

From a wide range of hollow fiber modules developed for various TFF applications (e.g., bioreactor perfusion, concentration, diafiltration, and clarification), eight commercially available membranes were selected and characterized for virus retention, DNA and protein contamination removal, and filter fouling. If available, a small- and large-pore

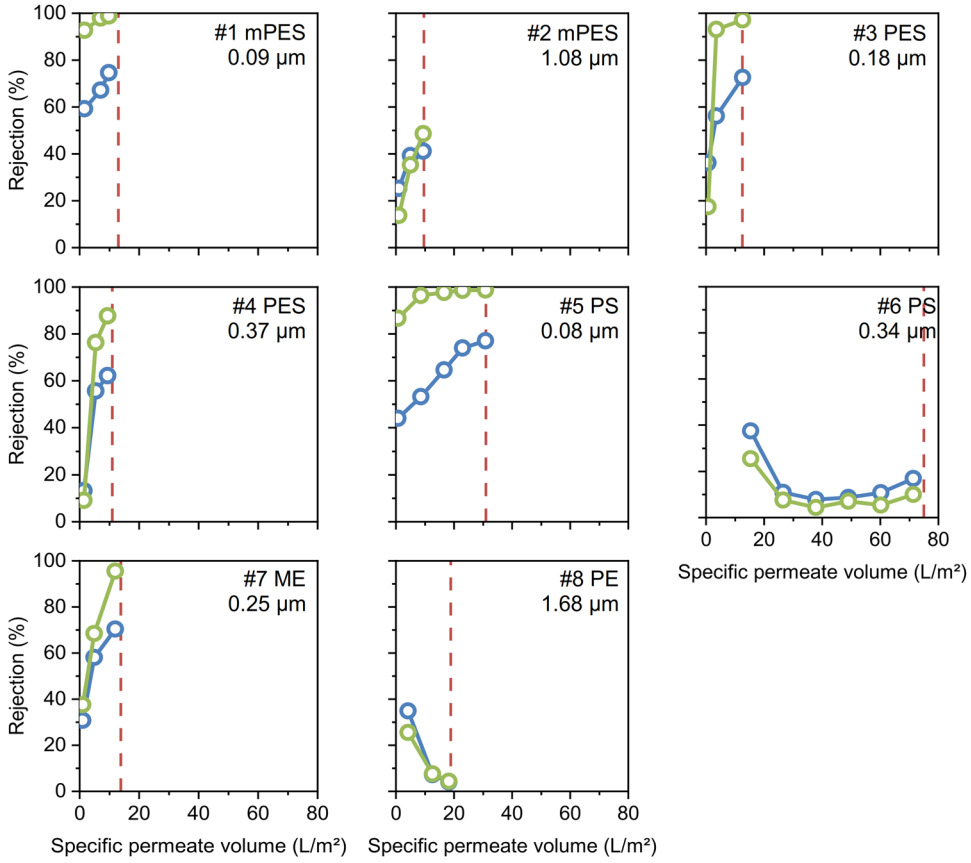

FIGURE 5 Percentage DNA and protein rejection of different hollow fiber membranes tested for continuous virus harvesting during perfusion operation. Contamination levels were determined from the supernatant of infected BHK-21$_{SUS}$ cells growing in BGM medium. DNA and protein samples were taken from the bioreactor vessel and permeate. Increments of DNA (green circle) and protein concentrations (blue circle) were expressed as rejection coefficients. Red dotted vertical line indicates complete membrane blockage. BHK-21$_{SUS}$, suspension-adapted baby hamster kidney cell; BGM, basal growth medium; ME, mixed ester; mPES, modified polyethersulfone; PE, polyethylene; PES, polyethersulfone; PS, polysulfone [Color figure can be viewed at wileyonlinelibrary.com]

membrane was selected from the same filter material to better understand the impact of the material or the measured cutoff on virus retention. While small-pore membranes can be suitable to accumulate the product in the bioreactor, large-pore membranes can potentially be employed to continuously harvest virions (for YFV ~50 nm). In both cases, it is desired to keep filter fouling to a minimum as it terminates the filtration process, and potentially ends in a complete product loss.

4.1 | Impact of general and physicochemical membrane properties on membrane fouling

To evaluate the impact of general and physicochemical membrane properties on membrane fouling and membrane blockage, observations were classified to predict their potential impact on membrane fouling. A high fiber thickness, a narrow pore size distribution and a high repulsion of foulants are considered to reduce filter fouling, while large pores allow general virus permeability (Table 4).

An increased fiber wall thickness is generally assumed to decrease permeate fluxes per driving force. In addition, a large contact surface allows for the adsorption of colloids, whereas intramembranous fluxes are increased in porous membranes that reduce membrane fiber blockage. The pore size distribution of membranes can be controlled to a certain extent by the manufacturing process, but is typically characteristic for the used material (Zeman & Zydney, 2017). For the PES, PS, and ME membranes, the 90th percentile of all pores was in a distinct range of about 25% in relation to the cutoff. The large-pore mPES and PE membranes, however, spread above 47%. Heterogeneous pore distributions are considered more susceptible to fouling as significant variation in filtrate flux along the length of the module occur, which turns large pores with higher local fluxes prone for concentration polarization and deposition until pore blockage. Thus, narrow pore size distributions have a uniform flux distribution and are generally considered better suited for long-term filtration operation (Jonsson, 1985; Table 4). The zeta potential was determined to assess repulsion effects. In theory, similarly charged colloids beyond the critical zeta potential (magnitude of ~10 mV) are repulsive and reduce filter cake formation desirable (Breite, Went, Prager, & Schulze, 2016; Cai et al., 2016). Thus, an advantageous repulsive effect for all tested membranes

TABLE 4 Structural and physicochemical membrane properties and their potential impact on membrane fouling

Membrane (µm)	Fiber thickness	Pore size[a]	Pore size distribution	Repulsion of foulants with membrane
1 mPES (0.09)	○	–	○	+
2 mPES (1.08)	○	+	–	+
3 PES (0.18)	○	○	+	+
4 PES (0.37)	○	+	–	+
5 PS (0.08)	○	–	+	+
6 PS (0.34)	–	+	+	+
7 ME (0.25)	○	○	○	+
8 PE (1.68)	–	+	–	?

Note: Increased fiber thickness, narrow pore size distribution, and high repulsion (based on zeta potential measurements) are considered to reduce filter fouling. Properties are categorized in (–) unfavorable, (○) neutral, (+) beneficial, or (?) unknown for reduced fouling. The more (+), the less susceptible to fouling and the better the membrane.

[a]Based on the pore size, membranes are grouped for virus permeability following – < ○ < +.

(measured at similar salt conditions) and the culture broth (measured at operating conditions) can be expected at pH 7.2 (Table 4). It should be noted that the zeta potential of the membranes was measured at lower salt concentrations, while the filtration was done under broth conditions with high salinity. It can be assumed that the streaming potential during filtration was lower than measured but values appear to correlate to the zeta potential of the culture broth (Breite et al., 2016; Schäfer, Pihlajamäki, Fane, Waite, & Nyström, 2004). Finally, measured membrane cutoffs allowed to group each membrane as strong virus-rejecting membrane (≤0.09 µm; mPES and PS), average rejecting membrane (0.25 µm; PES and ME), and low rejecting membrane (≥0.34 µm; mPES, PES, PS, and PE; Table 4).

4.2 | Impact of membrane structures on membrane fouling

SEM imaging revealed significant structural differences of tested membrane materials, and properties can be equally assessed regarding their potential fouling behavior (Table 5). While a high roughness of the inner membrane surface can hinder direct pore blocking (steric exclusion of particles and nonflush deposition on highly fissured surfaces), a reduced overflow velocity in valley-like structures can equally enhance deposition (Marshall, Munro, & Trägårdh, 1993). Such loose deposits are particularly sensitive for cake compression, when negative pressure on the permeate side increases (Vrijenhoek, Hong, & Elimelech, 2001). This could be assumed especially for mPES membranes, which additionally possess a high specific surface area that potentially enhances particle adsorption. Deep valley-like pore channels, as observed for the PE membrane, and narrowed pores are also unfavorable due to enhanced particle entrapment and membrane blockage. In contrast, the PS membrane (0.34 µm) has a very smooth material and open pore structure, as well as a high overall porosity so that foulants can freely penetrate the membrane, but are finally retained in deeper, more dense layers. This can enable high initial fluxes, but as deposits enrich within the membrane and physical countermeasures (e.g., increased flow velocity and backflushing) may not allow to overcome corresponding problems, full blockage will be inevitable. A size-selective and flat membrane surface, as observed especially for small-pore PS, but also for PES and ME membranes, enables thin boundary layers and optimum abrasive effects of the surface velocity (Choi, Zhang, Dionysiou, Oerther, & Sorial, 2005). This reduces concentration polarization (tendency for accumulation of foulants). However, if the surface porosity is low, such filters can react sensitive on pore narrowing with increasing membrane resistance. In dependence on the pore size and the size of foulants, small-pore membranes (in the range of ultrafiltration application) may be even less affected by fouling due to steric exclusion for pore narrowing or pore blocking (i.e., 0.08 µm PS membrane).

TABLE 5 Structural membrane properties (based on SEM imaging) and their potential impact on membrane fouling

# Material (µm)	Material roughness	Surface porosity	Pore structure	Surface roughness	Overall porosity
2 mPES (1.08)	–	?	–	–	+
3 PES (0.18)	○	○	○	+	○
5 PS (0.08)	+	–	○	+	–
6 PS (0.34)	+	+	+	○	+
7 ME (0.25)	–	○	○	+	○
8 PE (1.68)	+	–	–	○	–

Note: Only a reduced selection of most important membranes could be assessed via SEM imaging while covering the broad availability of materials used in biotechnological applications. Low material roughness, high surface porosity, open pore structure, low surface roughness, and high overall porosity are considered to reduce fouling. Properties are categorized in (–) unfavorable, (○) neutral, (+) beneficial, or (?) unknown for reduced fouling. The more (+), the less susceptible to fouling and the better the membrane.

Abbreviations: ME, mixed ester; mPES, modified polyethersulfone; PE, polyethylene; PES, polyethersulfone; PS, polysulfone; SEM, scanning electron microscope.

Overall, the large-pore PS membrane seems to combine suitable physicochemical and structural properties that can lead to a higher resistance against filter fouling, while enabling continuous virus permeability.

4.3 | Membrane fouling dynamics and its impact on product retention

To confirm previous assumptions on properties for filter fouling and virus retention, all membranes were tested consecutively in the same experimental setup in bioreactor perfusion mode. Each filtration experiment was performed once to ensure stable process conditions (e.g., cell broth pH, cell viability, and virus titer) throughout the test period. Therefore, conclusions or inferences should not be drawn from minor variations in the dynamics of the membrane resistance without looking at the entire set of membranes more as categories based on their structural and physicochemical properties. For those categories, there are repeated factors allowing a detailed interpretation. An immediate increase of membrane resistance is likely due to a combination of concentration polarization (reversible accumulation of rejected particles in the boundary layer) and a short period of deposition. The fast progression of fouling for both mPES membranes is potentially due to their rough material and surface promoting immediate deposition. Wide pore size distributions lead to an early blockage of larger pores, and accelerate subsequent blocking of smaller ones (Cho, Amy, & Pellegrino, 2000; Cornelissen, 1997). The increasing TMP (data not shown) compresses the filter cake, leading to full membrane blockage (Rana & Matsuura, 2010). A similar fouling tendency was observed for the small-pore PES membrane with low porosity. High permeate fluxes narrow scattered pores on the surface causing a quick reduction in the pore size, filter cake compression, and full blockage (Trzaskus et al., 2015). The short plateau in the development of membrane resistance for large-pore PES and ME membranes is, most likely, due to an equilibrium between deposition and foulant removal by overflow velocity until deposition dominates and the flux finally collapses. The PE membrane blocks potentially due to pore constriction and substantial pore closure. Interestingly, the PS membranes block only at notably high specific permeate volumes making them a candidate for long-term filtration operation. The fouling progression indicates an initial pore narrowing for the small-pore membrane, and an extended equilibration phase between deposition and foulant removal. The large-pore PS membrane with high porosity seems to be hardly affected by initial foulant-membrane adsorption and pore narrowing. Its relatively high membrane thickness (approximately four times larger than other membranes) did not noticeably contribute to lower intrinsic permeability. Instead, it seems to provide a larger effective separation surface area contributing to a better resistance against overall filter fouling. The round-shaped material structure enables high fluxes across and within the membrane and mitigates adhesion of foulant particles. However, due to its asymmetric membrane structure and pore narrowing, an irreversible particle deposition in deeper layers of the membrane can eventually not be avoided (Henry & Brant, 2012; F. Wang & Tarabara, 2008). This is in agreement with SEM imaging of the blocked membrane. While a strong cake is formed on fast fouling membranes such as mPES, PES, and ME, the large-pore PS membrane does not exhibit any obvious foulants on the surface (Figure S6, note that specimens were dried for observation, so that actual height of the cake layer could even have been greater during filtration operation). Therefore, foulants may be expected to be present at high quantities in deeper membrane structures. Notably, the observed membrane fouling progression is in close agreement with findings obtained for microfiltration processes (Trzaskus et al., 2015; Xiao, Shen, & Huang, 2013). It should be noted that the fouling of membranes is strongly linked to the material and process conditions tested. In accordance to the intrinsic membrane permeability (e.g., pore sizes, density, and physicochemical properties), optimal flow velocities and permeate fluxes can vary to achieve homogeneous fluxes along and through the membrane. Suboptimal conditions can otherwise favor local deposition and accelerate the progress of fouling.

Having understood fouling principles for the different membranes, product retention can be directly associated with membrane fouling dynamics. In the case of DNA and protein concentrations, here considered as impurities, their percentage rejection increased, possibly due to steric exclusion in narrowing pore channels, and increased repulsion from adsorbed foulants. Interestingly, the overall rejection was significantly higher for DNA than for proteins. Notably, the percentage rejection with PS (0.34 μm) and PE (1.68 μm) membranes showed a contrary trend. This observation may be explained by initial adsorption of DNA and protein to the membrane materials. Once the adsorptive membrane capacity is reached, impurities may migrate unimpaired through the large-pore channels into the permeate (Cornelissen, 1997). Hence, the use of PS membranes can be equally important for related perfusion processes where expressed proteins are considered as product, but retained by PES membranes with a nominal cutoff of 0.2 μm (Karst, Serra, Villiger, Soos, & Morbidelli, 2016; Kelly et al., 2014). Alternatively, other studies identified the use of large-pore membranes of 2 μm and larger as a solution for production retention (Pinto, Napoli, & Brower, 2019; S. B. Wang, Godfrey, Radoniqi, Lin, & Coffman, 2019). However, based on presented results, it is not the nominal cutoff but the membrane material and its associated properties that are of primary importance for membrane fouling and continuous product harvest via the permeate. Of results reported for the PES and PE membranes, the 0.34 μm PS membrane may be equally suitable for the continuous harvest of recombinant proteins and viral vectors.

5 | CONCLUSION

Our results highlight the importance of choosing the right membrane for intensified virus production and continuous product harvesting. We show that a selection based solely on nominal membrane pore size values reported by manufacturers may not be sufficient. Instead,

membrane material and associated structural and physiochemical properties are decisive factors that determine filter fouling and eventually the "true" membrane pore size causing product retention. The widely used PES (0.18 µm measured cutoff) membrane fouled quickly, so that YFV titers but also protein concentrations decreased rapidly in the permeate flow. In contrast, the 0.34 µm PS membrane was highly permeable for YFV particles and enabled continuous product harvesting in small-scale hollow fiber modules and TFF mode. In this context, different process conditions (e.g., flow velocity and permeate flux) and filtration operations (e.g., hydrodynamic backflushing, inverting flow directions, and pulsed flow) can be investigated to improve performance of the PS-based perfusion processes even further.

ACKNOWLEDGMENTS

The authors thank Bob Siemerink for SEM imaging and Iske Achterhuis from the Faculty of Science and Technology (University of Twente) for technical support and assistance in membrane characterization.

NOMENCLATURE

γ	s^{-1} shear rate at membrane wall
η_m	mPa s dynamic viscosity of medium
σ_{reject}	rejection coefficient
A	m^2 total filtration surface area
C_p	PFU/ml or µg/ml YFV, DNA or protein concentration in permeate flow
C_v	PFU/ml or µg/ml YFV, DNA or protein concentration in bioreactor vessel
f_n	number of hollow fibers
J	L/hr/m^2 surface-specific permeate flux rate
r	mm inner fiber lumen radius
R	m^{-1} total resistance
V	L maximum permeate volume
$\dot{V}_f$	ml/min volumetric flow rate
V_p	L/m^2 membrane-specific fouling capacity
$\dot{V}_p$	L/hr permeate flow rate

ORCID

Alexander Nikolay http://orcid.org/0000-0003-4475-9556
Joris de Grooth https://orcid.org/0000-0003-1553-768X
Yvonne Genzel https://orcid.org/0000-0002-2652-5943
Jeffery A. Wood https://orcid.org/0000-0002-9438-1048
Udo Reichl https://orcid.org/0000-0001-6538-1332

REFERENCES

Bielser, J. M., Wolf, M., Souquet, J., Broly, H., & Morbidelli, M. (2018). Perfusion mammalian cell culture for recombinant protein manufacturing—A critical review. *Biotechnology Advances*, *36*(4), 1328–1340. https://doi.org/10.1016/j.biotechadv.2018.04.011

Bolton, G. R., & Apostolidis, A. J. (2017). Mechanistic modeling of the loss of protein sieving due to internal and external fouling of microfilters. *Biotechnology Progress*, *33*(5), 1323–1333. https://doi.org/10.1002/btpr.2514

Breite, D., Went, M., Prager, A., & Schulze, A. (2016). The critical zeta potential of polymer membranes: How electrolytes impact membrane fouling. *RSC Advances*, *6*(100), 98180–98189. https://doi.org/10.1039/C6RA19239D

Cai, H., Fan, H., Zhao, L., Hong, H., Shen, L., He, Y., … Chen, J. (2016). Effects of surface charge on interfacial interactions related to membrane fouling in a submerged membrane bioreactor based on thermodynamic analysis. *Journal of Colloid and Interface Science*, *465*, 33–41. https://doi.org/10.1016/j.jcis.2015.11.044

Castilho, L. R., & Medronho, R. A. (2002). Cell retention devices for suspended-cell perfusion cultures. In K. Schügerl & A. P. Zeng (Eds.), *Tools and applications of biochemical engineering science* (pp. 129–169). Berlin, Heidelberg: Springer.

Cho, J., Amy, G., & Pellegrino, J. (2000). Membrane filtration of natural organic matter: Factors and mechanisms affecting rejection and flux decline with charged ultrafiltration (UF) membrane. *Journal of Membrane Science*, *164*(1), 89–110. https://doi.org/10.1016/S0376-7388(99)00176-3

Choi, H., Zhang, K., Dionysiou, D. D., Oerther, D. B., & Sorial, G. A. (2005). Influence of cross-flow velocity on membrane performance during filtration of biological suspension. *Journal of Membrane Science*, *248*(1), 189–199. https://doi.org/10.1016/j.memsci.2004.08.027

Cornelissen, E. R. (1997). *Membrane fouling in waste water filtration: Causes, consequences and prevention* (Doctoral thesis). University of Twente, Netherlands.

Fairbrother, F., & Mastin, H. (1924). Studies in electro-endosmosis Part I. *Journal of the Chemical Society*, *125*, 2319–2330.

Futselaar, H. (1993). *The transverse flow membrane module. Construction, performance and applications* (Doctoral thesis). University of Twente, Netherlands.

Gallo-Ramirez, L. E., Nikolay, A., Genzel, Y., & Reichl, U. (2015). Bioreactor concepts for cell culture-based viral vaccine production. *Expert Review of Vaccines*, *14*(9), 1181–1195. https://doi.org/10.1586/14760584.2015.1067144

Genzel, Y., Vogel, T., Buck, J., Behrendt, I., Ramirez, D. V., Schiedner, G., … Reichl, U. (2014). High cell density cultivations by alternating tangential flow (ATF) perfusion for influenza A virus production using suspension cells. *Vaccine*, *32*(24), 2770–2781. https://doi.org/10.1016/j.vaccine.2014.02.016

Henry, C., & Brant, J. A. (2012). Mechanistic analysis of microfiltration membrane fouling by buckminsterfullerene (C60) nanoparticles. *Journal of Membrane Science*, *415-416*, 546–557. https://doi.org/10.1016/j.memsci.2012.05.042

Hiller, G. W., Clark, D. S., & Blanch, H. W. (1993). Cell retention-chemostat studies of hybridoma cells – Analysis of hybridoma growth and metabolism in continuous suspension culture in serum-free medium. *Biotechnology and Bioengineering*, *42*(2), 185–195. https://doi.org/10.1002/bit.260420206

Jonsson, G. (1985). Molecular weight cut-off curves for ultrafiltration membranes of varying pore sizes. *Desalination*, *53*(1), 3–10. https://doi.org/10.1016/0011-9164(85)85048-7

Karst, D. J., Serra, E., Villiger, T. K., Soos, M., & Morbidelli, M. (2016). Characterization and comparison of ATF and TFF in stirred bioreactors for continuous mammalian cell culture processes. *Biochemical Engineering Journal*, *110*, 17–26. https://doi.org/10.1016/j.bej.2016.02.003

Kelly, W., Scully, J., Zhang, D., Feng, G., Lavengood, M., Condon, J., … Bhatia, R. (2014). Understanding and modeling alternating tangential flow filtration for perfusion cell culture. *Biotechnology Progress*, *30*(6), 1291–1300. https://doi.org/10.1002/btpr.1953

Marshall, A. D., Munro, P. A., & Trägårdh, G. (1993). The effect of protein fouling in microfiltration and ultrafiltration on permeate flux, protein retention and selectivity: A literature review. *Desalination*, *91*(1), 65–108. https://doi.org/10.1016/0011-9164(93)80047-Q

Nikolay, A., Castilho, L. R., Reichl, U., & Genzel, Y. (2018). Propagation of Brazilian Zika virus strains in static and suspension cultures using Vero and BHK cells. *Vaccine*, *36*(22), 3140–3145. https://doi.org/10.1016/j.vaccine.2017.03.018

Nikolay, A., Léon, A., Schwamborn, K., Genzel, Y., & Reichl, U. (2018). Process intensification of EB66® cell cultivations leads to high-yield yellow fever and Zika virus production. *Applied Microbiology and Biotechnology*, *102*(20), 8725–8737. https://doi.org/10.1007/s00253-018-9275-z

Pinto, N. D. S., Napoli, W. N., & Brower, M. (2019). Impact of micro and macroporous TFF membranes on product sieving and chromatography loading for perfusion cell culture. *Biotechnology & Bioengineering*, *117*, 117–124. https://doi.org/10.1002/bit.27192

Radoniqi, F., Zhang, H., Bardliving, C. L., Shamlou, P., & Coffman, J. (2018). Computational fluid dynamic modeling of alternating tangential flow filtration for perfusion cell culture. *Biotechnology and Bioengineering*, *115*(11), 2751–2759. https://doi.org/10.1002/bit.26813

Rana, D., & Matsuura, T. (2010). Surface modifications for antifouling membranes. *Chemical Reviews*, *110*(4), 2448–2471. https://doi.org/10.1021/cr800208y

Schäfer, A. I., Pihlajamäki, A., Fane, A. G., Waite, T. D., & Nyström, M. (2004). Natural organic matter removal by nanofiltration: Effects of solution chemistry on retention of low molar mass acids versus bulk organic matter. *Journal of Membrane Science*, *242*(1), 73–85. https://doi.org/10.1016/j.memsci.2004.05.018

Swan, J. W., & Furst, E. M. (2012). A simpler expression for Henry's function describing the electrophoretic mobility of spherical colloids. *Journal of Colloid and Interface Science*, *388*(1), 92–94. https://doi.org/10.1016/j.jcis.2012.08.026

Tapia, F., Vázquez-Ramírez, D., Genzel, Y., & Reichl, U. (2016). Bioreactors for high cell density and continuous multi-stage cultivations: Options for process intensification in cell culture-based viral vaccine production. *Applied Microbiology and Biotechnology*, *100*, 2121–2132. https://doi.org/10.1007/s00253-015-7267-9

Trzaskus, K. W., de Vos, W. M., Kemperman, A., & Nijmeijer, K. (2015). Towards controlled fouling and rejection in dead-end microfiltration of nanoparticles – Role of electrostatic interactions. *Journal of Membrane Science*, *496*, 174–184. https://doi.org/10.1016/j.memsci.2015.06.047

Ulbricht, M., Richau, K., & Kamusewitz, H. (1998). Chemically and morphologically defined ultrafiltration membrane surfaces prepared by heterogeneous photo-initiated graft polymerization. *Colloids and Surfaces*, *138*(2), 353–366. https://doi.org/10.1016/S0927-7757(98)00236-2

Vrijenhoek, E. M., Hong, S., & Elimelech, M. (2001). Influence of membrane surface properties on initial rate of colloidal fouling of reverse osmosis and nanofiltration membranes. *Journal of Membrane Science*, *188*(1), 115–128. https://doi.org/10.1016/S0376-7388(01)00376-3

Walther, J., McLarty, J., & Johnson, T. (2018). The effects of alternating tangential flow (ATF) residence time, hydrodynamic stress and filtration flux on high-density perfusion cell culture. *Biotechnology and Bioengineering*, *116*, 320–332. https://doi.org/10.1002/bit.26811

Wang, F., & Tarabara, V. V. (2008). Pore blocking mechanisms during early stages of membrane fouling by colloids. *Journal of Colloid and Interface Science*, *328*(2), 464–469. https://doi.org/10.1016/j.jcis.2008.09.028

Wang, S., Godfrey, S., Ravikrishnan, J., Lin, H., Vogel, J., & Coffman, J. (2017). Shear contributions to cell culture performance and product recovery in ATF and TFF perfusion systems. *Journal of Biotechnology*, *246*, 52–60. https://doi.org/10.1016/j.jbiotec.2017.01.020

Wang, S. B., Godfrey, S., Radoniqi, F., Lin, H., & Coffman, J. (2019). Larger pore size hollow fiber membranes as a solution to the product retention issue in filtration-based perfusion bioreactors. *Biotechnology Journal*, *14*(2), 1800137. https://doi.org/10.1002/biot.201800137

Wickramasinghe, S. R., Kalbfuß, B., Zimmermann, A., Thom, V., & Reichl, U. (2005). Tangential flow microfiltration and ultrafiltration for human influenza A virus concentration and purification. *Biotechnology and Bioengineering*, *92*(2), 199–208. https://doi.org/10.1002/bit.20599

Xiao, K., Shen, Y., & Huang, X. (2013). An analytical model for membrane fouling evolution associated with gel layer growth during constant pressure stirred dead-end filtration. *Journal of Membrane Science*, *427*, 139–149. https://doi.org/10.1016/j.memsci.2012.09.049

Zeman, L. J., & Zydney, A. L. (2017). Membrane formation technologies. *Microfiltration and ultrafiltration: Principles and applications*. Cleveland, OH: CRC Press. https://doi.org/10.1201/9780203747223

SUPPORTING INFORMATION

Additional supporting information may be found online in the Supporting Information section.

How to cite this article: Nikolay A, Grooth Jd, Genzel Y, Wood JA, Reichl U. Virus harvesting in perfusion culture: Choosing the right type of hollow fiber membrane. *Biotechnology and Bioengineering*. 2020;117:3040–3052. https://doi.org/10.1002/bit.27470